UC Berkeley
UC Berkeley Previously Published Works

Title
High spatial resolution Raman thermometry analysis of TiO2 microparticles

Permalink
https://escholarship.org/uc/item/9p87f7vt

Journal
Review of Scientific Instruments, 84(10)

ISSN
0034-6748

Authors
Lundt, Nils
Kelly, Stephen T
Rödel, Tobias
et al.

Publication Date
2013-10-01

DOI
10.1063/1.4824355

Peer reviewed

High spatial resolution Raman thermometry analysis of TiO2 microparticles

Nils Lundt, Stephen T. Kelly, Tobias Rödel, Benjamin Remez, Adam M. Schwartzberg et al.

Additional information on Rev. Sci. Instrum.

High spatial resolution Raman thermometry analysis of TiO$_2$ microparticles

Nils Lundt,[1,2] Stephen T. Kelly,[1] Tobias Rödel,[1,2,3] Benjamin Remez,[4,5]
Adam M. Schwartzberg,[4] Alejandro Ceballos,[6] Chloé Baldasseroni,[6] Peter A. F. Anastasi,[7]
Malcolm Cox,[7] Frances Hellman,[8] Stephen R. Leone,[1,2,8] and Mary K. Gilles[1,a]

[1]*Chemical Sciences Division, Lawrence Berkeley National Laboratory, Berkeley, California 94720, USA*
[2]*Department of Chemistry, University of California, Berkeley, California 94720, USA*
[3]*CSNSM, Universit Paris-Sud and CNRS/IN2P3, Bâtiments 104 et 108, 91405 Orsay Cedex, France*
[4]*Material Sciences Division, Lawrence Berkeley National Laboratory, Berkeley, California 94720, USA*
[5]*Racah Institute of Physics, Hebrew University, Jerusalem 91904, Israel*
[6]*Department of Materials Science and Engineering, University of California, Berkeley, California 94720, USA*
[7]*Silson Ltd, Northampton, England*
[8]*Department of Physics, University of California, Berkeley, California 94720, USA*

A new technique of high-resolution micro-Raman thermometry using anatase TiO$_2$ microparticles (0.5–3 μm) is presented. These very high spatial resolution measurements (280 nm) reveal temperature gradients even within individual microparticles. Potential applications of this technique are demonstrated by probing the temperature distribution of a micro-fabricated heater consisting of a thin silicon nitride (Si-N) membrane with a gold coil on top of the membrane. Using TiO$_2$ microparticle micro-Raman thermometry, the temperature from the outer edge of the coil to the inner portion was measured to increase by $\sim$40 $^\circ$C. These high spatial resolution microscopic measurements were also used to measure the temperature gradient within the 20 μm wide Si-N between the gold heating coils. 2D numerical simulations of the micro heater temperature distribution are in excellent agreement with the experimental measurements of the temperatures. These measurements illustrate the potential to extend applications of micro-Raman thermometry to obtain temperature details on a sub-micrometer spatial resolution by employing microparticles. © *2013 AIP Publishing LLC*.
[http://dx.doi.org/10.1063/1.4824355]

I. INTRODUCTION

In the fields of microelectrical and microelectromechanical systems, with steadily increasing device performance and decreasing feature sizes, thermal design and management are of great significance. Since heat dissipation is a limiting factor for many micro devices, improved ways of understanding heat transfer on a microscopic level are required. However, for micro devices with state-of-the-art feature sizes, it is challenging to characterize the thermal properties with conventional thermometry methods such as infrared (IR) emission[1] or contact-mode techniques.[2] The spatial resolution of IR-emission based methods is diffraction limited to about 10 μm.[1] In contact-mode methods, a fine probing thermometer tip, normally consisting of a thermocouple, is brought into contact with the sample and the tip temperature is read out. Although contact-mode methods can provide high spatial resolution ($\sim$20 nm), local heat transfer to the probe tip results in distorted temperature measurements and the temporal resolution is limited.[2] Therefore, new techniques such as micro-Raman or thermoreflectance thermometry have been developed for high spatial resolution thermometry (0.5 μm).[3] Micro-Raman thermometry uses the temperature dependent changes of spatially resolved Raman spectra.[4] By analyzing the Raman spectra, acquired by raster scanning the laser, a temperature distribution image with spatial resolution down to about 0.5 μm is obtained.[4] Although this is a diffrac-

tion limited technique, the shorter wavelength of the probe laser, as compared to IR emission, improves the spatial resolution. Micro-Raman thermometry has been used on microelectromechanical systems,[5–7] microelectronic devices,[8,9] optoelectronic systems,[10] and even in micro-fluidic channels.[11] Materials investigated by micro-Raman thermometry include various semiconductors such as silicon,[7] GaN,[9] GaAs,[12] and graphene.[13] However, in all of these applications the probed device is limited to specific materials such as semi-conductors and insulators. Materials such as metals are not well-suited to this technique because their very low phonon energies make it difficult to distinguish the Raman scattered light from the excitation source. In addition, the spectral characteristics of the probed material must be sensitive to temperature changes with a reasonably strong Raman scattering cross section, which further limits the applicable materials. Additionally, thermally induced stresses in the sample device affect the phonon mode energies. As a consequence, the spectral characteristics used to derive temperature are subject to strong cross correlations between temperature and strain. Thus, the temperature measurement may be distorted by thermally induced strain.

Microparticles with a strong and temperature-sensitive Raman signal, such as anatase (TiO$_2$),[14] can be used to map out the temperature at different device locations or alternatively, can be used to monitor the particle temperature. The latter is of interest for *in situ* particle or thin film investigations. To illustrate the potential for mapping temperature gradients, we employ a micro heater. Micro heaters are used for *in situ* experiments such as catalytic reactions on

a)Electronic mail: MKGilles@lbl.gov

nanoparticles[15] and microcalorimetry measurements.[16] These heaters typically consist of a metal heating coil at the center of membrane that is selected to be a poor thermal conductor to isolate the heated area from the environment. Often, these operate with the assumption that the temperature is the same on the active heating element, the membrane in regions without the heating element, and any material on either of these components. However, materials heated on very thin and transparent membranes in *in situ* TEM[17] and X-Ray microscopy[15,18,19] measurements may not exhibit the same temperature as the heating source. In fact, spatial characterization of the temperature distribution across such a heating device used in air showed a significant gradient across the membrane.[19] Therefore, a direct and contact-free particle temperature measurement with high spatial resolution is a valuable way to quantify the observed properties. Micro-Raman thermometry can show if the heating device provides uniform particle, device, or film heating, and reveal any temperature gradients within each of these.

In this paper, a new implementation of micro-Raman thermometry using microparticles (0.5–3 μm) deposited on the device is presented. The microparticles allow one to probe features of the device and serve as an indicator for the underlying substrate temperature at different positions with significantly higher spatial resolution than most current techniques. Unlike methods that directly probe an integrated device, this method is not restricted to specific substrate materials since Raman scattering from the microparticles on the device provides the measured data.

We briefly summarize the fundamental mechanisms of micro-Raman thermometry and present the basic principle and experimental details of the microparticle implementation. The latter includes the experimental setup, sample preparation, calibration, and spectral analysis for microparticle micro-Raman thermometry. Furthermore, we investigate sub-micrometer temperature distributions within individual microparticles. To illustrate temperature mapping of a device, we then examine a micro heater and quantify temperature heterogeneities across the heater and within the 20 μm gaps between the heater coils. 2D numerical simulations of the micro heater temperature distribution are compared with the high resolution temperature measurements. These measurements can provide insight into heat transfer and thermal gradients within and across materials at the sub-micrometer length scale and provide a benchmark for thermal simulations.

II. FUNDAMENTAL MECHANISM AND BASIC PRINCIPLE

Raman thermometry is based on the analysis of the inelastic energy transfer from an incident photon (probing laser beam) to a phonon (quantum of lattice vibration) in the specimen material, resulting in an outgoing photon at different energy. This inelastic energy transfer, the Raman effect, is temperature dependent. Therefore, it can be used to deduce the local specimen temperature. More specifically, the peak position, line width, and Stokes/anti-Stokes intensity ratio of the Raman spectrum vary with temperature. Although, each spectral characteristic depends on a different underlying physical

mechanism, each can be used to derive temperature. The selected approach depends on the temperature range of interest, experimental ease of data acquisition, and the potential of other effects to influence the spectral features.[4] Here, due to the experimental ease, we deduce temperature from the Raman peak position. The linear relation as well as the qualitative nature of the peak position measurements makes this approach attractive from a practical perspective. In addition, the shifts in peak position and the Raman scattering cross section are both strong for anatase.[14]

In general, the shift in peak position, $\Delta\omega$, with temperature results from a change in phonon energy. The phonon energy depends on lattice vibration frequencies that vary with interatomic forces. These are affected by the lattice expansion and contraction as the crystal is heated and cooled. This effect originates from anharmonicity in the bonding potential.[20] Aside from this volumetric effect, phonon-phonon interactions produce peak position shifts. The mere presence of a phonon alters the equilibrium spacing of atoms in the lattice, affecting interatomic forces. Consequently, the phonon energy of both this phonon and other phonons is changed. Ultimately, the shift in peak position is enhanced relative to the pure volumetric effect.[4] Over the typical operation range of many micro devices (0–200 °C), the relation between temperature and shift in peak position can be described by a linear function given by

$$\Delta\omega = A(T - T_0), \tag{1}$$

where A is a calibration constant that describes the linear relation between peak position and temperature T, whereas T_0 is the base temperature corresponding to a known peak position. The detailed description of the calibration is given in Subsection III B. The temperature is obtained from the Raman peak position (ν_6 (E_g) mode) using this calibration and finally, temperature images of the microparticles are generated. Additionally, any effects influencing interatomic forces such as thermo-elastically induced or externally applied strain interfere with the temperature measurement. Strain effects are expected to be minimal in our configuration as particles loosely applied to the surface can freely expand and contract during cooling and heating.

III. EXPERIMENTAL

A. Instrumental setup

The instrument is based on a confocal Raman microscope (WiTec alpha300, schematically illustrated in Figure 1), coupled with a continuous mode Nd:YAG laser (λ = 532 nm). The laser mode is coupled by a single-mode optical fiber and a holographic grating into the light path of the microscope where it is focused by a 50× or a 100× objective. For the 100× objective with a numerical aperture of 0.95, the theoretical resolution limit according to the Bragg diffraction limit would be 280 nm. The sample is mounted on a piezo stage that enables precise scanning. The scattered light, coupled into a multi-mode optical fiber, is analyzed and detected by a spectrometer equipped with a CCD camera. An appropriate laser power adjustment provides a strong signal without
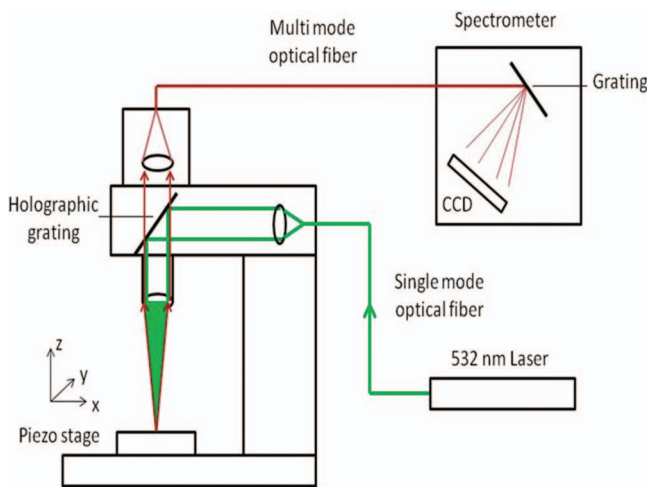
FIG. 1. Experimental setup of the confocal Raman microscope. The probing laser beam is coupled through a single mode optical fiber into the microscope pathway and is focused on the micro heater surface. The micro heater is mounted on a piezo stage that can be scanned. The Rayleigh scattered light is blocked by a holographic grating in the detection pathway and only the Raman scattered light is coupled through a multi mode optical fiber to the spectrometer.

heating the microparticles. This illustrates an additional requirement for the microparticle material: the bandgap must be larger than the corresponding energy of the probing photons. This reduces interband photon absorption and minimizes laser-induced heating. Here, the bandgap of anatase (3.20 eV) is sufficiently larger than the probing photon energy (1.95 eV). Another consequence of the large bandgap is the transparency of anatase and high penetration depth for the probing light. Despite the low absorption, we investigated the influence of laser power on the ν_6 (E$_g$) phonon mode peak position. The peak position serves as an indicator for probe laser induced heating. The experimental results presented in Figure 2 for anatase particles in air on a silicon nitride membrane demonstrate that for laser powers >2 mW, the peak position shifts to higher wavenumbers, a strong indication of laser-induced particle heating. Therefore, all laser scans in
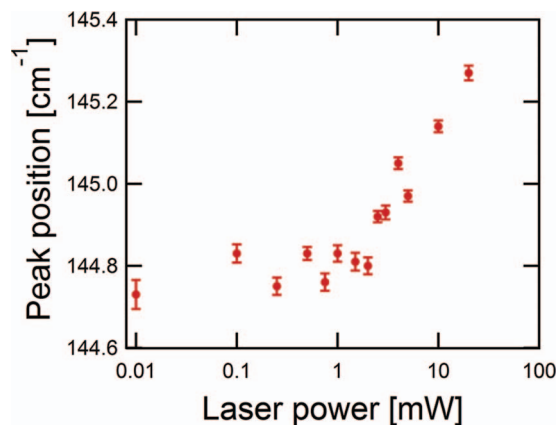

FIG. 2. Fitted ν_6 (E$_g$) phonon peak position of anatase plotted as a function of the probe laser power. The peak position remains constant up to a laser powers of 2 mW. At higher laser powers, the peak position shifts indicating laser-induced heating.
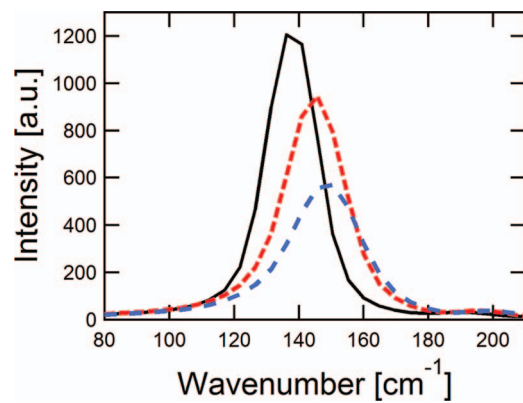

FIG. 3. Raman spectra of the anatase ν_6 (E$_g$) phonon peak acquired at 22 °C (solid line), 270 °C (dashed line), and 510 °C (dashed line with larger spacing). The peak position clearly shifts to higher wavenumbers as the temperature increases.

this work were carried out at 1 mW with the exception of the microparticle scans described in Sec. IV.

B. Data processing and calibration

The Raman signal at each point on the micro heater surface (pixel) is analyzed by fitting its ν_6 (E$_g$) phonon mode peak with a Gaussian function

$$f = a\,exp\left(-\left(\frac{x-b}{2c}\right)^2\right), \qquad (2)$$

where a, b, and c are fitting parameters. Fitting parameter b is equivalent to the peak position of the phonon peak and is used to derive temperature from the Raman signal. Figure 3 displays the spectra of the ν_6 (E$_g$) phonon mode measured at several temperatures. At higher temperatures, the peak broadens and shifts to higher wavenumbers. This observation is in agreement with previous investigations[14] and the theoretically predicted behavior described above. A quantitative analysis provides the calibration required to relate the measured peak position to temperature. For the calibration, anatase microparticle powder (in ambient air) was heated uniformly by a button heater, probed by a thermocouple, and the ν_6 (E$_g$) peak position was measured at various temperatures. The relation between peak position and temperature is fitted with Eq. (1), where A is the fitting parameter obtained from the calibration. Subsequently, A is used to relate the peak position to temperature.

However, obtaining an accurate calibration was challenging due to uneven thermocouple and powder heating and potential cooling effects. When the powder and thermocouple tip were both in contact with the button heater but not in direct contact with each other, the calibration results were not reproducible. This configuration overestimates temperature and underestimates A, since the thermocouple tip is more efficiently heated than the micro powder. Good powder-thermocouple contact was critical for the calibration to ensure an identical powder and thermocouple temperature. By depositing the anatase powder with a tweezer tip directly onto the junction area of the K type thermocouple, and gently pressing the tip, reproducible results for the calibration were obtained.
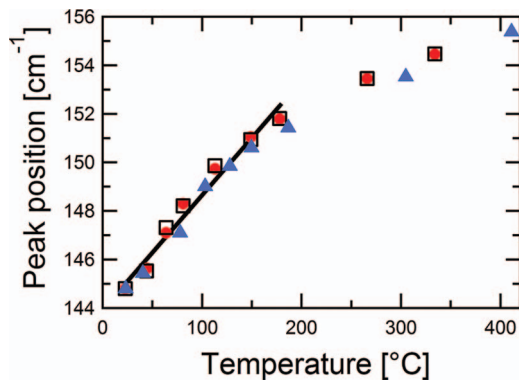
FIG. 4. Fitted ν_6 (E_g) phonon peak position of anatase plotted as a function of sample temperature (error bars are within data point symbols). Different symbols correspond to separate calibrations. In the temperature range up to 180 °C, the data points can be fitted with Eq. (1) resulting in a calibration constant A of 0.0472 cm^{-1}/°C.

To improve the statistics for the calibration, a 50 μm × 50 μm area, covering several thousand particles, was scanned. The button heater located underneath the thermo-couple provided the heating. An aluminum foil shield sur-rounding the button heater minimized air convection. With the powder and thermocouple tip in direct contact, the devi-ation between powder and thermocouple tip temperature is expected to be minimal, and very reproducible results are ob-tained (Figure 4, A = 0.0472 cm^{-1}/°C fitted in the range up to 200 °C, standard deviation of 0.90 × 10^{-3} cm^{-1}/°C). This value is relatively high compared to other materials of interest such as silicon, which has an A value of 0.021–0.024 cm^{-1}/°C.[3,5,6,8] The ν_6 (E_g) peak position of anatase is much more sensitive to temperature changes than the phonon modes of many other materials; thus it is excellent for temper-ature characterization in this temperature range. As previously reported[14] and shown in Figure 4, at temperatures higher than 200 °C a quadratic contribution dominates the peak position-temperature relation.

IV. MICROPARTICLE ANALYSIS

The high spatial resolution of the confocal micro-Raman setup allows the investigation of temperature gradients within individual microparticles. Single particle scans also provide information about the spatial resolution limit of this micro-Raman thermometry implementation. In high resolution (20 nm step size) single particle measurements, anatase mi-croparticles about 1 μm in diameter deposited on the surface of a button heater were scanned with a step size of 20 nm at room temperature (22 °C) and at 90 °C. To enhance the low signal-to-noise ratio, the probing laser power was adjusted to 5 mW. The identical particle was also scanned at 1 mW laser power with a five-fold integration time. The comparison con-firms that the influence of laser-induced heating was low and consistent with the results in Figure 2. Figure 5(a) presents the temperature image of a selected anatase microparticle at room temperature. The sharp and well defined particle edges arise from an applied signal intensity threshold to cut-off sig-nal contributions (due to the diffraction-limited laser beam di-ameter) outside the particle boundary.
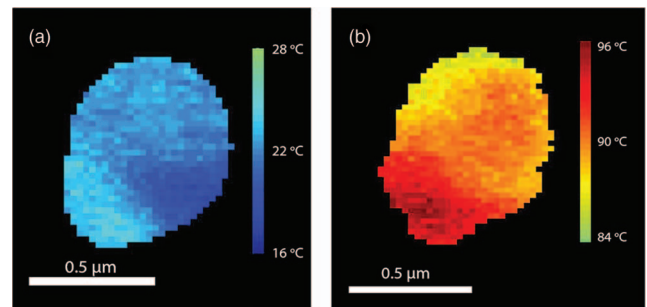

FIG. 5. Temperature map of a 1 μm diameter TiO$_2$ microparticle scanned with 20 nm step size at 22 °C (a) and at 90 °C (b).

Surprisingly, although a homogeneous temperature dis-tribution is expected at room temperature, the measured tem-perature in the particle ranges from 18 °C up to 24 °C (6 °C gradient). At room temperature, any influences on interatomic forces, such as internal strain, defects, or differences between particle grains, will shift the phonon peak position. These ef-fects would manifest as temperature gradients that may not exist and will limit the thermal accuracy of this technique, or could potentially be a way to measure and quantify effects such as strain.

When the identical particle is heated to 90 °C (Figure 5(b)) a similar temperature distribution within the particle (from 86 °C to 94 °C or 8 °C gradient) is ob-served. In contrast to the room temperature scan, a general decrease in temperature from the center of the particle to the outer edge is seen in Figure 5(b). This additional gradient is attributed to cooling from the surrounding gas. Both of these gradients (differences in the internal particle structure and air cooling) influence the measured temperature distribution of the heated particle.

The images in Figure 5 reveal the high spatial resolution of this technique. Despite the diffraction-limited laser beam diameter, features of a few hundred nanometers are resolved, approaching the theoretical resolution limit of 280 nm. This high resolution results from the confocal setup of the micro-scope which reduces background signal coming from material volume outside the focal plane, combined with the sensitivity of the anatase peak position to temperature.

The thermal accuracy is limited by three contributions: the fitting uncertainty for the Raman peak position, un-certainty of the calibration constant, and internal particle structure that affects the peak position. The temperature un-certainty due to the fitting error (assuming sufficient signal-to-noise ratio) is ±0.6 °C. The uncertainty in the calibration constant, A, is 1.9% of the difference between the measured temperature and room temperature. The uncertainty related to internal particle structure can be calculated from the stan-dard deviation of the average particle temperature. However, this standard deviation also contains actual temperature varia-tions such as cooling effects or laser-induced heating. Con-sequently, this uncertainty can only be estimated from this microparticle analysis to be ±2 °C. Overall, the total temper-ature accuracy is estimated to be ±3–5 °C.

Since particles used in this study have a broad size (0.5–3 μm) and shape distribution and may consist of aggregates of smaller particles, the heat transfer (and dissipation) can

vary depending upon particle size and morphology. These dependencies explain the temperature variations of particles that might be expected to be isothermal according to simulation results. If particles of a uniform shape and monodisperse size were used, more uniform particle heating might be measured. However, most of the synthetic focus on TiO_2 is to create nanoparticles too small for micro-Raman measurements. Hence, ideal microparticles (spherical and monodisperse in the size range 0.5–1.5 μm) are not readily available. However, recent investigations indicate that improving existing micro-Raman thermometry setups could increase signal-to-noise ratios,[21] making microparticles smaller than 0.5 μm potentially accessible for this type of implementation.

V. MICRO HEATER CHARACTERIZATION

To illustrate the potential for high spatial resolution temperature probing, anatase microparticles were used to determine the temperature on a micro-heating device. Due to their transmission properties, thin Si-N membranes are frequently used for soft X-ray and electron beam microscopies and have been used as a substrate for *in situ* micro reactors. The very low thermal conductivity of Si-N membranes allows good insulation between the center of the membrane and the microscope environment, but also limits thermal conduction in the sample area. Despite the importance of accurate knowledge of temperature for *in situ* experiments, many studies assume that, because of the close proximity of the heating device and sample, their temperatures are identical and do not consider the limited heat conduction.[15,17,18]

The prototype heater (0.5 × 0.5 mm) from Silson, shown in Figure 6(a), consists of a freestanding, 200 nm thick Si-N window (0.7 × 0.7 mm) supported by a silicon chip. A gold coil (150 nm thick with 20 μm spacing between coil elements) is deposited on the Si-N membrane for resistive heating. These device dimensions as well as the size range of typically investigated particles (0.5–10 μm) require high spatial resolution characterization techniques. Sample heating and heat loss from the heater occur through the emitted heat radiated from the gold coil, by thermal conductance from the coil through the Si-N membrane, and thermal conduction and convection through the surrounding gas. Radiation from the gold wires is also expected to be minimal due to the low emissivity of gold (0.085)[19] but could be more significant for other metals.

To obtain a uniform and sufficiently dense particle distribution, TiO_2 powder (Aldrich, anatase, 325 mesh, 99% trace metal basis) was sonicated in ethanol for 15 min and centrifuged (VWR Galaxy Mini centrifuge) for 90 s. Small particles remain dispersed in the ethanol and larger particles sediment at the bottom of the centrifuge tube. The dispersion, containing particles from 0.2 to 3 μm, was spin-coated onto the micro heater surface. During spin-coating, particles smaller than 0.5 μm aggregate to form larger secondary particles. The particles are dispersed sufficiently to minimize thermal conductance between them.

Figure 6(b) presents the temperature image of a small coil section (25 × 25 μm) indicated in Figure 6(a). The Raman spectral images were acquired with a step size of 0.2 μm and
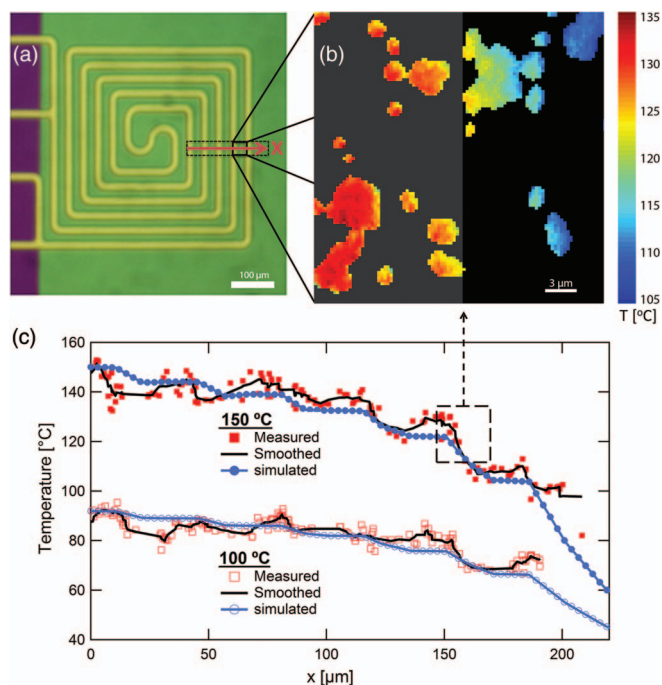

FIG. 6. (a) Schematic illustration of micro heating device (Silson Ltd) consisting of a Si-N membrane (200 nm, green) and a gold coil (150 nm, yellow). Sections scanned for (b) and (c) are indicated. (b) Temperature image of selected coil area during heating at 32.4 mW. Grey background indicates gold coil, black background the Si-N membrane. (c) Average temperatures of single particles across the heater as a function of their position in x-direction (red squares, error bars are within data point symbols). The simulated temperature profiles are indicted with connected, blue dots. The two profiles correspond to heating at 12.7 mW and at 32.4 mW, respectively.

an applied electrical power of 32.4 mW. The average particle temperature was calculated as the mean value of all pixels within an individual particle. The particle edges were defined by setting a threshold for the Raman signal intensity. Because the fitting uncertainty is largest for the smallest particles, average temperatures from particles larger than 0.5 μm were used to determine the temperature gradient on the micro heater. In general, the heated microparticles appear to be cooler at their edges than in their center. Particles closest to the inner coil (dark grey background in Fig. 6(b)) are warmer than those particles furthest to the right in Fig. 6(b). Using anatase microparticles on the micro heater, on average, the gold coils were measured to be (12–15 °C) warmer than the neighboring Si-N regions. The heat transfer to particles in the spacing between coil wires is limited by conduction through the Si-N membrane. This is in contrast to the direct heat transfer between the gold to the particles on the coil wires.

To illustrate the ability of the microparticle method to provide details on the temperature distribution over a device such as the micro heater, a rectangular area (225 × 25 μm), perpendicularly aligned to the coil wires (indicated in Figure 6(a)), was imaged at two different electrical power settings (12.7 mW and 32.4 mW). Figure 6(c) displays the particle average temperatures (red squares) as a function of position in the x-direction. As seen in Figure 6(c), the temperature of the micro heater increased from the outermost to the innermost coil (∼40 °C at 32.4 mW and ∼20 °C at 12.7 mW). Superimposed on this is an oscillating pattern of high

temperature on the gold heating coil and a decrease in temperature at the center of the Si-N region. These experiments indicate at least four temperature gradients: gradients within individual particles, variations within the spacing between the heating coils, the temperature difference between coil wire and silicon nitride membrane regions, and the overall gradient across the micro heater.

VI. MICRO HEATER TEMPERATURE SIMULATION

Microparticle temperature measurements can also serve as a benchmark for theoretical simulations of heat transfer. To illustrate this, similarly to previously reported work,[19] 2D numerical simulations at two input powers were carried out for the micro heater temperature distribution. These simulations consider three heat transfer processes: blackbody radiation, thermal conduction through the membrane and surrounding air, and convection through the air. No heat transport to or from the microparticles is considered. The simulation solves the two-dimensional partial differential heat equation in the steady state of the micro heater:

$$-\nabla * (k_{2D}\nabla u) + hu + \sigma\epsilon\big((u + u_0)^4 - u_0^4\big) = P_{2D}, \quad (3)$$

where u_0 is the base temperature (for example, room temperature), u is the temperature increase relative to base temperature, k_{2D} is the two-dimensional thermal conductivity in W/K, h is the convection heat transfer coefficient in W K^{-1} cm^{-2}, σ is the Stefan-Boltzmann constant, ϵ is the emissivity, and P_{2D} is the two-dimensional power dissipated by the heater in W/cm^2.[19] The first term describes conduction through the membrane and gold wires, where the two-dimensional thermal conductivities are assumed to add in parallel. The second and third terms refer to air convection/conduction and blackbody radiation, respectively. h is a coefficient determined by empirical correlations[22] that approximates convection and conduction through the surrounding air.

Experimental input powers, 12.7 mW and 32.4 mW, were used for P_{2D}. The value of k_{2D}(Si-N) (2.434 × 10^{-6} W/K) was determined by linearly interpolating literature results for the thermal conductivity of Si-N membranes of similar thicknesses.[19,23] Then, the heater's average temperature was determined by measuring its resistance at the two operating powers (121 Ω at 12.7 mW and 163 Ω at 32.4 mW), together with a resistance-temperature (R(T)) measurement of the coils (homogeneously heated in an oven). Finally, using correlation methods[22] an initial value for h was calculated, which was subsequently refined until the simulation yielded an average temperature that matched the one calculated from the results of the R(T) measurement. The optimized values for h were 0.08 for 12.7 mW and 0.12 for 32.4 mW.

Figure 7 shows the overall temperature distribution simulation of the micro heater operated at 32.4 mW. The indicated temperature profiles in Figure 7 (also plotted in Figure 6(c)) are in excellent agreement with the microparticle Raman thermometry measurements. Both measured and simulated micro heater temperatures exhibit the same trends: the temperature increases from the outer edge of the coil to the inner portion, the gold coils are warmer than the neighboring Si-N regions,
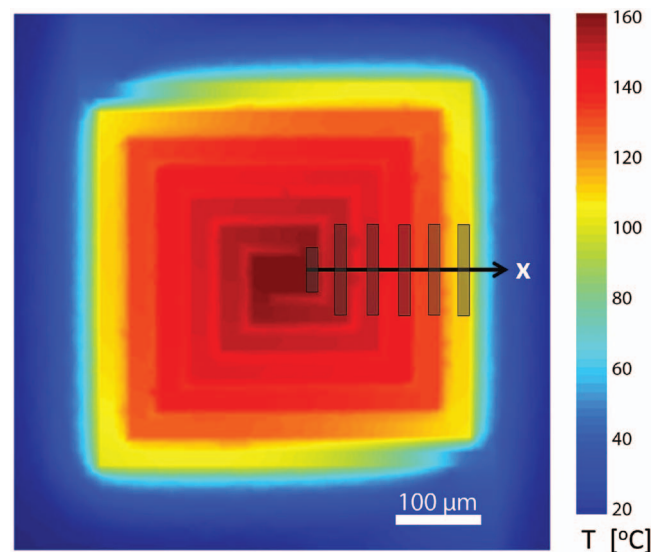

FIG. 7. Simulated temperature distribution of micro heater operated at 32.4 mW. The profile indicated by the arrow is plotted in Figure 6 at two temperatures. The locations of the gold wire along this path are indicated by grey boxes.

and a temperature gradient on the Si-N between sets of gold coils are observed. Note that the simulations provide temperatures for the device, whereas the measured temperatures are from particles on the membrane. The thermal conduction between particles and membrane could vary from particle to particle due to differences in particle morphology, which influences the thermal conduction between the two. For example, the simulation predicts that particles located a similar distance from a heating coil should have identical temperatures. However, the microparticle Raman thermometry measurements indicate variations up to ±5 °C for similarly located particles. As discussed in Sec. IV, the high spatial resolution experimental measurements indicate temperature gradients within individual particles that could result from internal strain, grain boundaries, or defects. Nevertheless, the numerical simulations are in excellent agreement with the measured temperatures and overall trends in the micro heater.

VII. SUMMARY

We developed a new implementation of micro-Raman thermometry using microparticles as a temperature probe. Anatase (TiO$_2$) microparticles were chosen due to their strong Raman-scattering and the high temperature sensitivity of their ν_6 (E$_g$) mode. Temperature images of individual microparticles with a spatial resolution of ~280 nm, approaching the diffraction limit, are obtained. These measurements indicate that temperature gradients exist within individual particles for unheated and heated particles. High spatial resolution scans revealed potentially interfering effects of intrinsic particle defects (i.e., strain) that could affect the peak position of the acquired Raman signal and, hence, temperature measurements. The use of a uniform shape and monodisperse microparticles on a nonreactive metal surface (high thermal conductance) or incorporating a thin conductive layer on the back of the Si-N

membrane[19] should reduce the temperature gradients of the micro heater. Heated particles were typically cooler around the edges than in the center, presumably from air-cooling.

This technique was applied to a micro heater to demonstrate the ability to map temperature gradients with a high spatial resolution. Temperature mapping was done by placing anatase microparticles on top of a device surface, a micro heater, and measuring the microparticle temperature. The micro heater temperature distribution was simulated and compared to the measured values. Both experiments and simulations show: (a) a temperature gradient present in the Si-N space between the heating coils; (b) the gold coil wires are warmer than the Si-N regions; and (c) the temperature in the center of the micro heater is higher than the outermost parts.

Compared with probing the embedded device material itself, this approach extends the range of investigable materials, it ensures a strong and temperature-sensitive Raman signal, and could reduce cross correlation errors due to thermally induced stresses. Since metal surfaces are not accessible with existing micro-Raman thermometry techniques, employing microparticles as a temperature probe will expand the use of micro-Raman thermometry techniques to these materials.

ACKNOWLEDGMENTS

[1] A. N. Smith and P. M. Norris, *Handbook of Heat Transfer* (John Wiley & Sons, Inc., New York, 2003).

[2] A. Majumdar, "Scanning thermal microscopy," Annu. Rev. Mater. Sci. **29**, 505 (1999).

[3] T. Beechem and S. Graham, "Temperature measurement of microdevices using thermoreflectance and Raman thermometry," in *BioNanoFluidic MEMS* (Springer, New York, 2008), Chap. 6, pp. 153–174.

[4] T. E. Beechem and J. R. Serrano, "Raman thermometry of microdevices: Comparing methods to minimize error," Spectroscopy Solutions for Materials Analysis **26**, 36 (2011).

[5] J. R. Serrano, L. M. Phinney, and S. P. Kearney, "Micro-Raman thermometry of thermal flexure actuators," J. Micromech. Microeng. **16**, 1128 (2006).

[6] M. R. Abel, T. L. Wright, W. P. King, and S. Graham, "Thermal metrology of silicon microstructures using Raman spectroscopy," IEEE Trans. Compon. Packag. Manuf. Technol. **30**, 200 (2007).

[7] T. Beechem, S. Graham, S. P. Kearney, L. M. Phinney, and J. R. Serrano, "Simultaneous mapping of temperature and stress in microdevices using micro-Raman spectroscopy," Rev. Sci. Instrum. **78**, 061301 (2007).

[8] R. Ostermeir, K. Brunner, G. Abstreiter, and W. Weber, "Temperature distribution in Si-MOSFETs studied by micro-Raman spectroscopy," IEEE Trans. Electron Devices **39**, 858 (1992).

[9] M. Kuball, G. J. Riedel, J. W. Pomeroy, A. Sarua, M. J. Uren, T. Martin, K. P. Hilton, J. O. Maclean, and D. J. Wallis, "Time-resolved temperature measurement of AlGaN/GaN electronic devices using micro-Raman spectroscopy," IEEE Trans. Electron Device Lett. **28**, 86 (2007).

[10] M. Kuball, J. W. Pomeroy, S. Rajasingam, A. Sarua, M. J. Uren, T. Martin, A. Lell, and V. Härle, "High spatial resolution micro-Raman temperature measurements of nitride devices (FETs and light emitters)," Phys. Status Solidi A **202**, 824 (2005).

[11] S. H. Kim, J. Noh, M. K. Jeon, K. W. Kim, L. P. Lee, and S. I. Woo, "Micro-Raman thermometry for measuring the temperature distribution inside the microchannel of a polymerase chain reaction chip," J. Micromech. Microeng. **16**, 526 (2006).

[12] A. Sarua, A. Bullen, M. Haynes, and M. Kuball, "High-resolution Raman temperature measurements in GaAs p-HEMT multifinger devices," IEEE Trans. Electron Devices **54**, 1838 (2007).

[13] I. Calizo, A. A. Balandin, W. Bao, F. Miao, and C. N. Lau, "Temperature dependence of the Raman spectra of graphene and graphene multilayers," Nano Lett. **7**, 2645 (2007).

[14] T. Ohsaka, "Temperature dependence of the Raman spectrum in anatase TiO_2," J. Phys. Soc. Jpn. **48**, 1661 (1980).

[15] E. de Smit, I. Swart, J. F. Creemer, G. H. Hoveling, M. K. Gilles, T. Tyliszczak, P. J. Kooyman, H. W. Zandbergen, C. Morin, and B. M. Weckhuysen, "Nanoscale chemical imaging of a working catalyst by scanning transmission x-ray microscopy," Nature (London) **456**, 222 (2008).

[16] D. W. Denlinger, E. N. Abarra, K. Allen, P. W. Rooney, M. T. Messer, S. K. Watson, and F. Hellman, "Thin film microcalorimeter for heat capacity measurements from 1.5 to 800 K," Rev. Sci. Instrum. **65**, 946 (1994).

[17] M. Zhang, E. A. Olson, R. D. Twesten, J. G. Wen, L. H. Allen, I. M. Robertson, and I. Petrov, "*In situ* transmission electron microscopy studies enabled by microelectromechanical system technology," J. Mater. Res. **20**, 1802 (2005).

[18] I. J. Drake, T. C. N. Liu, M. K. Gilles, T. Tyliszczak, A. L. Kilcoyne, D. K. Shuh, R. A. Mathies, and A. T. Bell, "An *in situ* cell for characterization of solids by soft x-ray absorption," Rev. Sci. Instrum. **75**, 3242 (2004).

[19] C. Baldasseroni, D. R. Queen, D. W. Cooke, K. Maize, A. Shakouri, and F. Hellman, "Heat transfer simulation and thermal measurements of microfabricated x-ray transparent heater stages," Rev. Sci. Instrum. **82**, 093904 (2011).

[20] G. Lucazeau, "Effect of pressure and temperature on Raman spectra of solids: anharmonicity," J. Raman Spectrosc. **34**, 478 (2003).

[21] C. B. Saltonstall, J. Serrano, P. M. Norris, P. E. Hopkins, and T. E. Beechem, "Single element Raman thermometry," Rev. Sci. Instrum. **84**, 064903 (2013).

[22] W. M. Rohsenow, J. P. Hartnett, and Y. I. Cho, *Handbook of Heat Transfer*, 3rd ed. (McGraw-Hill, New York, 1998).

[23] B. Revaz, B. L. Zink, and F. Hellman, "Si-N membrane-based microcalorimetry: Heat capacity and thermal conductivity of thin films," Thermochim. Acta **432**, 158 (2005).